Quantum interference in half-cycle microwave multiphoton transitions

C. W. S. Conover and J. H. Rentz
Physics Department, Colby College, Waterville, Maine 04901
(Received 26 September 1996)

We observe microwave multiphoton transitions in Rydberg states of Na using intense subnanosecond half-cycle electric field pulses in a microwave transmission line. Transition probabilities from n^*s and n^*d states, ranging in principal quantum number from 18 to 40, to nearby n^*l ($l \geq 2$) states are measured both as a function of pulse amplitude and the delay between two identical temporally spaced pulses. The transition rate depends strongly on both the pulse amplitude and the temporal delay between the two pulses. Nearly 100% of the population can be transferred for certain amplitudes of the half-cycle pulse. Transition probabilities are successfully described both with a dynamic Stark model and direct numerical integration of the time-dependent Schrödinger equation. Ramsey interference between two delayed pulses is observed that shows strong-field behavior. The two-pulse experiment is a technique for high-order multiphoton spectroscopy without concern for ac Stark shifts. [S1050-2947(97)05705-3]

PACS number(s): 32.80.Wr, 32.80.Rm

I. INTRODUCTION

There continues to be interest in the nonperturbative dynamics of both ground-state and Rydberg atoms influenced by strong time-dependent electric fields. Recent experiments and theoretical approaches have made the importance of coherence in multiphoton processes increasingly evident. Coherence in nonperturbative dynamics has become an important tool in the manipulation (control) of atomic and molecular transitions [1], as well as in cooling and trapping atoms through adiabatic passage [2]. Typical experiments on ground-state atoms have been performed using high intensity lasers, while significant efforts have been made in examining the multiphoton transitions and ionization of Rydberg atoms by electric fields of several different types. Ionization of Rydberg atoms with slowly ramped fields [3–5], microwave fields [6,7], and recently half-cycle THz [8] and GHz [9,10] pulses of field have all been studied.

We have explored the phase dependence of dynamics of Rydberg atoms driven by intense half-cycle pulses of electric fields, using both single pulses of varying amplitude and pairs of time-delayed pulses. With these experiments we hope to address questions of the field required for intermanifold population transfer in nonhydrogenic systems, and to measure the importance of coherence on these population transfers, particularly as this relates to microwave ionization. Previous models of microwave ionization treated the process as a sequence of incoherent steps, but recently Gatzke *et al.* [11] have shown for pulses of microwaves with only a few cycles that coherence is important in the population transfer.

In addition, these experiments are closely analogous to an ideal multiphoton ionization experiment, where transient multiphoton resonances can provide the dominant mechanism for ionization [12–14]. Coherence between excitation on the rising and falling edges of a laser pulse has been shown to be an important aspect to these processes [15,16]. The level dynamics in our system are similar to those seen in the Floquet picture of multiphoton ionization, but the experiments presented below are performed in a nearly uniform field. For this reason, they do not suffer from the disadvantage of averaging over focal volume that makes the measurement of coherence effects difficult.

The two-pulse experiments provide a system that is easy to understand with a simple theoretical model. They also provide a technique for multiphoton spectroscopy without ac Stark shifts. Spectroscopic measurements can be made in the range of MHz to THz using 1-GHz bandwidth half-cycle pulses. These results also give practical information on the importance of phase coherence over the many-cycle pulses of microwaves used in microwave ionization experiments.

We observe transitions between Rydberg states in sodium, ranging in principal quantum number from 18 to 40 driven by nearly unipolar impulses of electric field, called half-cycle pulses (hereafter HCP's), with a full width at half-maximum (FWHM) of 500 ps. In these experiments, the coherent bandwidth of the HCP's is significantly less than the energy level spacings at zero field, placing these experiments clearly in the realm of multiphoton transitions. For example, the energy spacing between the 27 s and 26 $l \geq 3$ states is 200 GHz, which corresponds to approximately 400 photons at the central frequency of the HCP spectrum. In addition, the experiments use low enough frequency radiation that the pulse amplitude and shape can be fully characterized, avoiding a problem with THz HCP's [8].

We compare the results of the experiment to predictions of a dynamic Stark model and direct integration of the Schrödinger equation. Many of the features of the data are readily understood using the dynamic Stark (Landau-Zener) picture of multiphoton transitions, which will be described in Sec. III A. The experiments are also reasonably easy to simulate with direct numerical integration because the number of interacting states is moderate. Quantum calculations were performed using a finite spherical basis; the Hamiltonian matrix was determined using standard numerical methods [17] and the known energy levels of the Na atom [18]. The Schrödinger equation was integrated using the Bulirsh-Stoer method [19]. For these calculations the HCP pulse shape is modeled as

$$F_1(t) = F_0 \sin^4\left(\pi \frac{t}{T}\right), \tag{1}$$

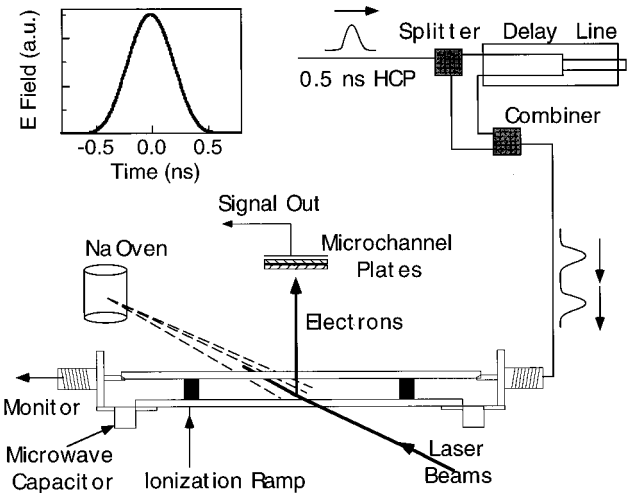

FIG. 1. Main features of the experimental apparatus showing the pulse delay scheme, parallel plate transmission line, atomic source, and microchannel plate detectors. The atomic and laser beams are antiparallel with the laser polarization in the vertical direction. The transmission line is constructed of brass with SMA connectors and 100-pF microwave capacitors used to couple the HCP onto the line while isolating the bottom plate from ground to allow a state-selective field ionization pulse to be applied. Several 0.7-mm holes drilled in the top plate of the transmission line allow electrons from the ionized atoms to reach the detector. Inset: the shape of the HCP used in the experiment.

where T is the full width of the field pulse and F_0 is the peak amplitude. For the numerical calculations a pulse in the form of Eq. (1) with $T=1.30$ ns matches the shape and width of the pulse measured in the laboratory.

Previously Lankhuijzen and Noordam [9] have directly observed this type of multiphoton transition between Rydberg states in Rb, using HCP's with nanosecond time scales. They saw that for 140-ps-wide pulses, population transfer takes place at the manifold mixing field $1/3n^5$, independent of the initial state [9]. For 9-ns-wide HCP's they were able to compare their results to numerical calculations of the transition probability for a digitized HCP. In both regimes of their experiments, the population transfer was never complete. The experiments presented below provide a second system on which to study these multiphoton transitions in a regime where the population transfer can be nearly 100% when driven by a single HCP.

In the following sections we present a description of the experimental arrangement, a summary of the results for both the thresholds for population transfer and the quantum interference in both single- and double-pulse experiments, a discussion of the dynamic Stark model of the multiphoton transitions, and our conclusions.

II. EXPERIMENT

We observe microwave HCP driven transitions in Rydberg states of Na in a molecular beam. A thermal beam of Na atoms from a resistively heated oven is created in a vacuum chamber with a background pressure of about 1×10^{-7} Torr. The beam passes through the center of a parallel plate transmission line, shown schematically in Fig. 1. The Na atoms are excited first from the $3s_{1/2}$ to the $3p_{1/2}$ state and then to selected Rydberg $n^*s_{1/2}$ or $n^*d_{3/2}$ states with $|m_j|=\frac{1}{2}$ by two home-built pulsed dye lasers pumped by the harmonics of a Nd:YAG (yttrium aluminum garnet) laser. A particular n^*s or n^*d state can be selected by changing the color of the second (blue) dye laser. About 100 ns after the Na atoms are excited by the two dye lasers, an HCP or a pair of HCP's are incident on the Rydberg atoms. Then, 200 ns after the HCP's, there is slow (2 μs) high-voltage ramp (peak field 8.0 kV/cm) applied to the ground side of the transmission line that ionizes any Rydberg states in the interaction region.

The transmission line is constructed of brass plates 3.81 cm wide, spaced by 0.508 cm and 30 cm long. The line has a nominal impedance of 50 Ω. The transmission line is coupled to coaxial cables on each end using a standard SMA connector as shown in Fig. 1, with the ground plate coupled via 100-pF microwave capacitors (American Technical Ceramics ATC-100). The capacitors allow the application of a high-voltage ramp to the ground side of the transmission line for state-selective field ionization. Care was taken to minimize the reflection of the HCP at the interface between the coaxial lines and the parallel-plate transmission line. The amplitude of the reflected pulse is measured by time-domain reflectrometry to be less than 7% of the pulse amplitude. This corresponds to a voltage standing wave ratio of less than 1.25. The length of the transmission line delays any reflection of the HCP at the SMA connectors until after the main pulse is past.

To reduce any state mixing by magnetic fields, the lasers are fired synchronously with the zero crossings of the line voltage. In addition, the transmission line is surrounded by an open-ended rectangular box constructed of mu-metal (Eagle Magnetic AAA) that is 2.5 in.^{2} and 15 in. long. The interaction region is also placed at the center of a pair of Helmholtz coils that are oriented vertically, which eliminate the majority of the earth's magnetic field in the interaction region. These precautions reduce the magnetic field in the interaction region to less than 0.1 G.

The HCP's are produced with an Avtech Electrosystems AVH-HV1 impulse generator, which produces 100-V pulses with a 500-ps FWHM. The output voltage of the pulser can be set using a control voltage provided by a computer-controlled digital-to-analog converter (DAC). For several of the experiments the pulse was additionally attenuated using broadband coaxial attenuators. The pulser can produce up to 150-V/cm pulses in the interaction region, with the reduction due to various losses in the cables and reflection.

Imperfections in the HCP come from two experimental considerations: field homogeneity and imperfections in the unipolarity of the HCP. Based on ramped field ionization curves of individual Rydberg states, the field homogeneity in the interaction region is estimated to be better than 1%. This homogeneity is important to observe interference effects since relative phases depend on the energy differences in the HCP field. The capacitors used to isolate the coaxial cable from the high-voltage field ionization pulse form a high-pass filter with the termination resistor that has a 3 dB frequency of 30 MHz, which gives a small, long, and negative tail to the pulse. This, along with the reflection of the pulse from the end of the transmission line, which is inverted, means that the pulse is not an ideal HCP.

The bottom plate of the transmission line is connected to a slowly ramped pulse from a trigger transformer circuit that can be used to selectively field ionize the atoms. Since each Rydberg state ionizes at a characteristic field and therefore at different times during the voltage ramp, the time of arrival of the electrons can be used to distinguish their state. Electrons produced by field ionization pass through one of several 0.7-mm holes in the top plate of the transmission line and are detected by microchannel plates. The microchannel plate signal is amplified and averaged in a boxcar integrator. The output of the boxcar integrator is read by a DAC and the data are transferred to a computer.

The detection scheme is highly selective for low-l states, but high-l states precess in the residual magnetic field into high-m states so that they are ionized diabatically by the ramped field. Because of the many m levels and the large numbers of small avoided crossings between states at high fields, it is very difficult to selectivity detect the population of the high-l states. For the most part we have measured the population in the initial state only and used the ionization of all atoms as a normalization. This careful normalization allows direct comparison with the population transfer predicted by numerical methods.

III. DATA

The data from two different experiments are presented below. In the first experiment, described in Sec. III A, the population transfer from initial n^*s and n^*d states to high-l states is measured as a function of peak electric field in an HCP. In the second experiment, discussed in Sec. III B, the population transfer is measured as function of the time delay between two HCP's.

A. Single HCP experiments

In the experiments described in this section the pulse splitting and combining apparatus shown in Fig. 1 was removed and the transmission line was directly connected to the HCP generator. The single pulse experiments were performed on n^*d states over the range of principal quantum numbers from 18 to 40. The experiments on the n^*s states, due to the larger HCP fields required, were performed over the range of principal quantum numbers from 26 to 40. The qualitative features of the n^*d and n^*s population transfer as a function of field are discussed first, a dynamic Stark picture of the multiphoton transitions is developed, and then the locations of thresholds for transitions and maxima of transition probability as a function of the principal quantum number are examined.

Figures 2 and 3 show typical results of population transfer versus HCP amplitude for a range of principal quantum numbers. In these figures, the experimental data are shown as discrete points and the solid lines are the results of numerical simulations based on the direct integration of the Schrödinger equation. The numerical simulations are in quantitative agreement with the experimental results within the experimental uncertainty in the pulse amplitude. Both Figs. 2 and 3 show that nearly 100% of the population can be transferred out of the initial state for certain pulse amplitudes. This shows that HCP's can be of significant use in control schemes. However, in these experiments there is not a single ''target'' state to which the population is transferred; that would require a sequence of HCP's.

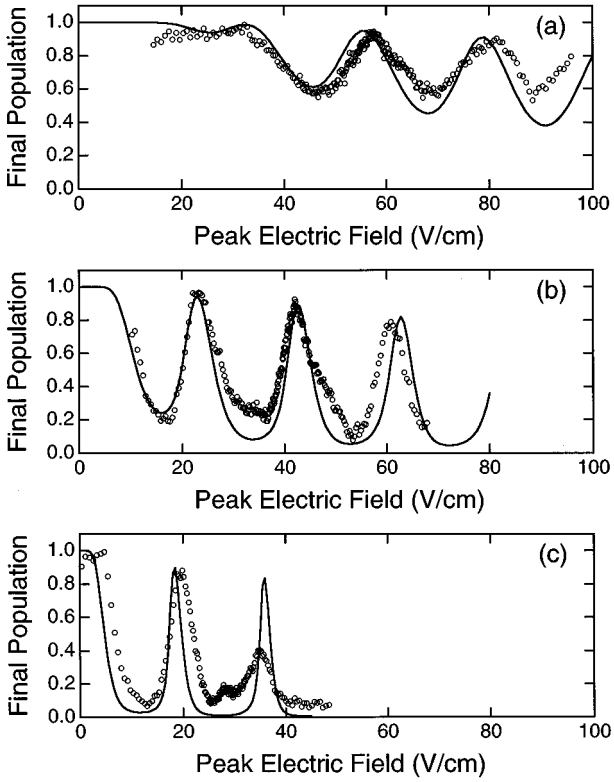

FIG. 2. Experimental (○) and computed curves (solid lines) of population in the (a) 21d, (b) 25d, and (c) 29d states versus peak amplitude after a single HCP. The computed curves were calculated using Schrödinger's equation on a limited basis.

The output of the AVH-HV1 is not calibrated, nor is it a linear function of the voltage input to its amplitude control. The HCP amplitudes were calibrated with two different methods. To calibrate the HCP amplitude in our scans of population transfer versus amplitude such as those shown in Figs. 2 and 3, the amplitude of the HCP is measured with a sampling oscilloscope. The pulse is observed using a 20-dB pulse coupler (Picosecond Pulse Labs Model 5520 C) before it enters the vacuum chamber, and again after it passes through the transmission line and again leaves the vacuum chamber. This method also gives a good measure of the pulse shape given in Eq. (1) and shown as an inset in Fig. 1. The uncertainties associated with this method of calibrating the amplitude of the pulse result in an estimated uncertainty of 5% in the pulse amplitude. To further confirm the calibration we apply several dc offset voltages to the bottom plate of the transmission line and observed the change in the peak HCP field required for the onset of the population transfer.

Population transfer between fine structure levels is important in the n^*d experiments, but is not displayed in these figures. Both the $n^*d_{3/2}$ and $n^*d_{5/2}$ populations were added together for the data presented in Fig. 2. The calculations were performed using the j basis and for the theoretical curves in Fig. 2, the $n^*d_{3/2}$ and $n^*d_{5/2}$ populations were added as in the experiment. Calculations were also performed in the l basis, and they agree with the calculations in the j basis if the $m_l=0$ and $m_l=1$ calculations are averaged.

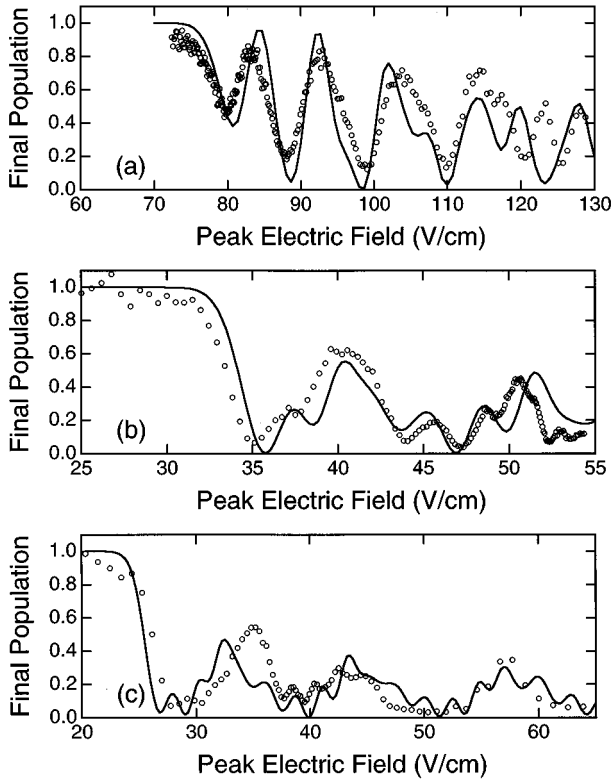

FIG. 3. Experimental (○) and computed curves (solid lines) of population in the (a) 29*s*, (b) 34*s*, and (c) 36*s* states versus peak amplitude after a single HCP. The computed curves were calculated using Schrödinger's equation on a limited basis.

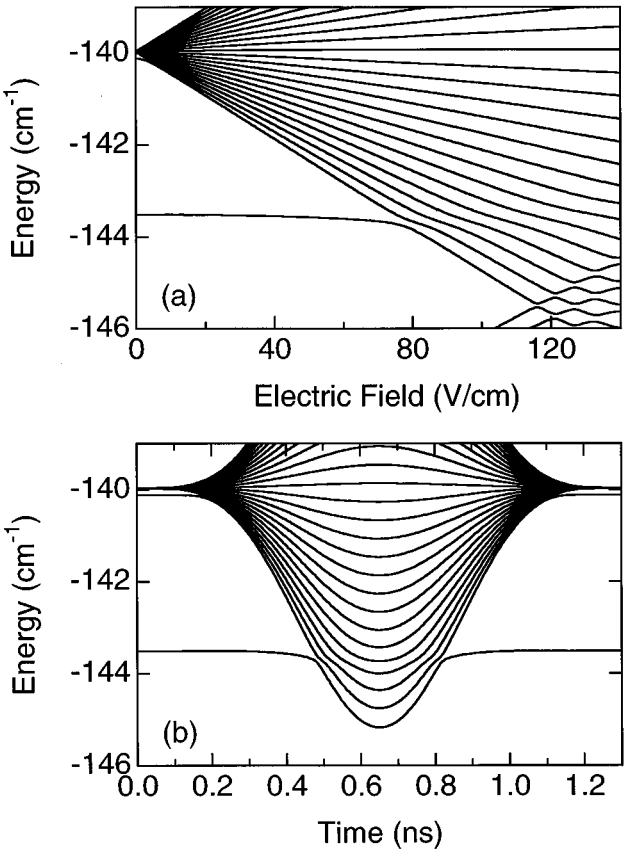

FIG. 4. (a) Energy level diagram versus electric field for Na near the 29*s* state and (b) a dynamic picture of the same states versus time in a microwave half-cycle pulse with a peak field of 110 V/cm and 500 ps FWHM.

While both sets of data show similar behavior, exhibiting ''thresholds'' for population transfer and several maxima and minima in the population transfer, there are qualitative differences aside from the voltage scale that should be noticed. The n^*d population versus HCP field is a smooth curve exhibiting several regularly spaced minima. The ''thresholds'' for population transfer are not sharp. The minima in the remaining population decrease in amplitude, indicating more population transfer out of the initial states as a function of peak HCP field. It should be noticed that all three curves in Fig. 2 are plotted on the same horizontal scale and that the features do not change rapidly with principal quantum number. Deviations from the theoretical curves at high HCP fields could be due to the fact that at these peak fields the 7% reflection of the HCP is large enough to drive transitions between all of the states.

The n^*s population, seen in Fig. 3, is a much less regular function of peak HCP field. The ''thresholds'' for population transfer are much sharper, with the *s*-state population decreasing rapidly as a function of HCP voltage. The spacing between individual minima is also not as regular, nor do the minima decrease monotonically in size with HCP amplitude. The data in Figs. 3(a)–3(c) are graphed on different scales, due to the rapid changes of the features with principal quantum number. Unlike in the n^*d experiments the n^*s state population is not disturbed by the reflected pulse even at the largest amplitudes studied because of the large threshold for population transfer.

Aside from the direct numerical integration of Schrödinger's equation, the features in the data and the differences between the data presented in Figs. 2 and 3 can be understood using a Landau-Zener model. Figure 4(a) shows an energy level diagram and the electric-field dependence of a typical set of Rydberg states near $n=28$ with $|m_l|=0$. Figure 4(b) shows a picture of these energy levels as a function of time during a 500-ps HCP. This dynamic Stark picture will illustrate the origin of the ''thresholds'' for population transfer and the role of coherence in the multiphoton transitions, using transitions between the 29*s* state and the $n=28$ $l\geqslant 2$ states as an example.

Initially, only the 29*s* state is populated. The $n=28$ $l\geqslant 2$ states shift their energies in the HCP field, so that several of them become degenerate with the state adiabatically connected to the 29*s* state at different times during the pulse. The states mix and do not cross, but rather form an avoided crossing that is traversed on both the rising and falling edges of the HCP, during which Landau-Zener transitions are made between two states. In a two-state Landau-Zener model, the population transfer between two states at an avoided crossing depends on both the avoided crossing size Ω_{ij} between the two states and the time rate of change of the uncoupled energies,

$$\dot{\omega}_{ij}=\frac{d}{dt}\,(W_i-W_j)=\frac{dW_{ij}}{dF}\,\frac{dF}{dt}, \tag{2}$$

in the vicinity of the crossing. As shown explicitly in Eq. (2), $\dot{\omega}_{ij}$ depends on two independent quantities, the rate of

change of the energy levels with the field, dW_{ij}/dF, and also on the rate of change of the field with time, dF/dt; these two quantities can independently affect the transition probability. The diabatic transition probability is given by [20]

$$P_{\text{diab}} = e^{-2\pi\Gamma_{ij}}, \tag{3}$$

where

$$\Gamma_{ij} = \frac{\Omega_{ij}^2}{4\dot{\omega}_{ij}}. \tag{4}$$

Equation (3) is only exact for constant $\dot{\omega}_{ij}$, but the expression has been extended by McIlrath *et al.* [21] to include higher-order terms, for times when the slew rate is changing. The simple expression is, however, adequate for discussion of the data.

Each Landau-Zener transition creates a coherent superposition of the different states, which then evolve at different frequencies. Between the avoided crossings in Fig. 4(b), the different states accumulate a relative dynamical phase

$$\Delta\Phi_{ij} = \frac{1}{\hbar}\int_{t_1}^{t_2} \Delta E_{ij}(t)\,dt, \tag{5}$$

where t_1 and t_2 are the times at the avoided crossings and ΔE_{ij} is the energy difference between the two states. This phase is the area in Fig. 4(b) bounded by any two energy levels and the avoided crossings.

Gatzke, Watkins, and Gallagher [22] have shown that for two symmetric avoided crossings, such as shown in Fig. 4(b), where Γ_{ij} is the same for both the rising edge and the falling edge of the pulse, that for a two-state problem, the probability of ending in the initial state after a HCP is

$$P_i = 1 - [4P_{\text{diab}}(1 - P_{\text{diab}})]\sin^2\left(\frac{\Delta\Phi}{2}\right). \tag{6}$$

The second term in Eq. (6) is a product of two factors, the first factor (in square brackets) is the result of the Landau-Zener model without considering coherence. The incoherent theory predicts a maximum transition probability when $P_{\text{diab}} = 0.5$. This factor describes the origin of the ''thresholds'' of population transfer seen in Figs. 2 and 3. There will be an onset of population transfer between the 29*s* state and the $l \geqslant 2$ states when the amplitude of the HCP equals the field of the static-field avoided crossing. The actual amount of population transferred will depend on the size of the avoided crossing and $\dot{\omega}_{ij}$ near the crossings. For large avoided crossings or small dW/dF there can be significant population transfer only for rapid slew rates, dF/dt, which occur in the middle of the HCP's rise and fall. For small avoided crossings or large dW/dF, there can only be significant population transfer for low slew rates, which occur near the peak of the pulse. In the intermediate regime large population transfers can occur during any part of the HCP.

For the principal quantum numbers studied, the sizes of the avoided crossings between the n^*d and the manifold state, which it first intersects, ranges from about 5 GHz at the lowest quantum numbers studied to about 0.25 GHz at $n = 40$. For the n^*s states the comparable avoided crossings range from 7 GHz at principal quantum number of 27 to 2 GHz at $n = 40$. Determining these avoided crossing sizes perturbatively with the method of Komarov, Grozdanov, and Janev [23] is difficult because they arise from the crossings of states isolated from the high-l states. Instead, the sizes were determined by numerically diagonalizing the Stark Hamiltonian using the method of Zimmerman *et al.* [17] The avoided crossings in both sets of states are comparable in size to the bandwidth of the HCP. Using this knowledge about the states and the model summarized in Eq. (6), the differences in the behavior of the thresholds between the n^*s and n^*d data will be discussed.

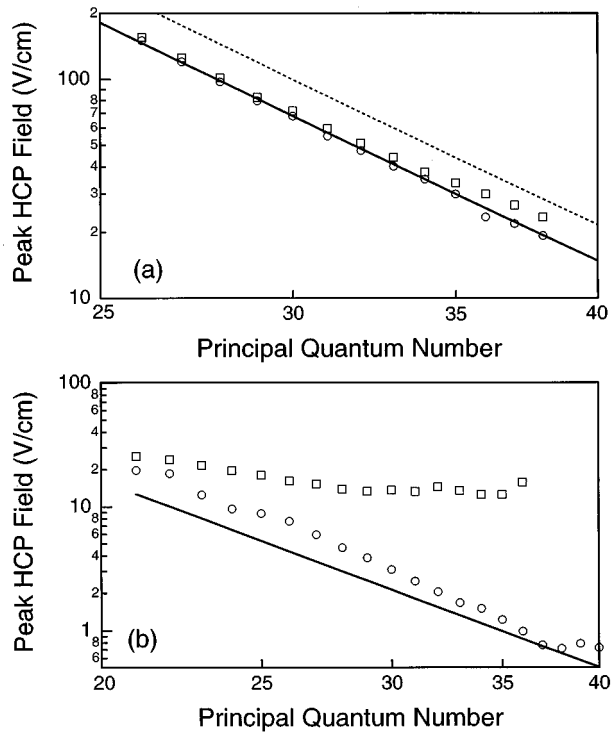

FIG. 5. Experimental and theoretical (solid lines) field values required for population transfer for initially populated *s* and *d* states as a function of n^*. Field required for the first maxima in population transfer (□) and for 10% of the first maxima (○) in the population transfer out of the (a) n^*s states and (b) n^*d states. The theoretical curves are based on the location of the initial avoided crossings in a static field as shown in Fig. 4(a).

A summary of the ''thresholds'' for multiphoton transitions are shown in Fig. 5, which is a plot of the measured peak HCP fields at the first maximum in population transfer to the high-l states from the initially populated states (□) and the peak HCP fields required to transfer 10% of the population in that first maximum (○). Also shown are the theoretical lines, determined from simple hydrogenic scaling laws, showing the static field of the first avoided crossing of the n^*d and n^*s states with the manifold (solid lines). Figure 5(a) also shows the field where the n and $n-1$ manifolds mix (dashed line). Because population is redistributed to many $l \geqslant 2$ states in these experiments and it is difficult to measure each state's population, Figs. 2 and 3 display the population of the initial states. However, for ''threshold'' measurements in the low-n states, where the population transfer within a single pulse is small, the high-l state population is much less susceptible to noise from laser or atomic

beam fluctuations than the initial state population, and for these measurements the high-l state population was used.

In Fig. 5(a), the thresholds for 10% population transfer are at the crossing of the n^*s state with the manifold: significantly below the n-state mixing field. The threshold data scales at $1/n^5$ as would be expected from the simple scaling law. The first maximum is very close to the 10% transfer field, which demonstrates that the thresholds are sharp. At higher principal quantum number, as the avoided crossings get smaller, the location of the first maximum in the population transfer moves relatively higher in voltage. In Fig. 5(b) the thresholds for the n^*d states are seen to be significantly above the crossing field at low n, moving closer to the crossing field at high n. The data scale as $1/n^{5.5}$, which also agrees with the simple scaling law. The field of the first maxima in Fig. 5(b) is much larger than the 10% transfer field, demonstrating that the n^*d thresholds are much less sharp than the n^*s thresholds.

Despite the fact that the n^*s avoided crossings are comparable in size to those in the n^*d experiments, the thresholds are much sharper. The diabatic transition probability defined in Eq. (3) demonstrates why. Despite the fact that the HCP is identical, dW/dF is much greater in the case of the n^*s states, which leads to a significantly smaller Γ_{ij}. So, for the n^*s states, even with the small slew rates near the peak of the pulse, P_{diab} can be large and a large population can be transferred to the high-l states. For the n^*d states, dW/dF is quite small at the avoided crossings, and the slew rate of the field, dF/dt, must become large for there to be significant population transfer. The deviation of the low-n n^*d ''thresholds'' from the simple scaling argument is likewise due to the small value of dW/dF for the n^*d states: there is a very small transition probability when the peak field of the HCP just equals the crossing field.

Lankhuijzen and Noordam [9] showed that for 140 ps FWHM pulses the 10% population transfer in Rb over the range $n^*=25-40$ for s, p, and d states took place at the field $1/3n^5$: the static field required for manifold mixing. Since this is the threshold field found in microwave ionization of nonhydrogenic atoms, it is surprising that the field is so consistent, independent of the initial states. Our data show that this consistency is merely a consequence of the pulse width and the atom chosen, where the p and d states are roughly midway between the two sets of high-l states. In Rb, none of the three lowest l states mix strongly with the manifold states (the avoided crossings are small) until the electric field reaches the manifold mixing regime. For the two pulse widths that they chose, they worked in either the nearly purely adiabatic or nearly purely diabatic regime for the crossings of the isolated states with the manifold. In Na, where the p and d states are close to the high-l states, there is a strong mixing of the s, d, and p states when they first intersect the manifold, which is at a field significantly less than the manifold mixing field. In the experiment presented here, the peak HCP fields required to drive transitions are roughly equal to the static fields required to reach the first avoided crossing with the manifold, not at $1/3n^5$.

One of the striking features of the data from Figs. 2 and 3 is that there are several relative minima in the initial-state population as a function of the peak HCP field. The oscillations in the data derive from the phase-dependent factor in Eq. (6), which shows that the population transfer between states depends on the relative phase of the states accumulated between multiple traversals of the same avoided crossing. Because of this term Stückelberg oscillations appear in the population transfer if either the energies or times between crossings are altered: both change with the HCP amplitude.

The shape of the n^*d data with HCP voltage is well described by the Landau-Zener model. For the lowest n states, such as the data shown in Figs. 2(a) and 2(b), the n^*d states have a small likelihood of population transfer at the avoided crossing because of the very small dW/dF at the crossings. Thus the experiment is nearly an ideal two-state problem and the populations show the $1-\sin^2(\Delta\Phi/2)$ behavior expected from Eq. (6). The amplitude of the modulation generally increases with peak HCP field as is expected from increasing P_{diab}. For higher principal quantum number as seen in Fig. 2(c) or larger slew rate as seen at the highest peak HCP fields in Fig. 2(b) the individual crossings are more diabatic and more than two states are involved. For the n^*d experiments, the avoided crossings are spaced so closely together that the individual Stückelberg oscillations overlap with each other; individual peaks are not seen and the result is a broadening out of the minima in the final population from the form expected in Eq. (6). This broadening is clearly observed in Fig. 2.

Figure 3(a), which has the largest avoided crossings of the data shown, shows that at low-peak HCP field, just above the threshold for population transfer, there is a set of three peaks which are regularly spaced. These peaks are not spaced in field with the locations of the multiple avoided crossings seen in Fig. 4(a). They are much more widely spaced indicating that they are also due to interference effects. As the peak HCP field increases the first avoided crossing is traversed more diabatically and a second series of interference peaks due to population transfer into more than one manifold state arises. The experiment progresses from a nearly two-state problem for the low-peak field case of Fig. 3(a) to the case in Fig. 3(c) where there are clearly many closely spaced peaks due to the nearly diabatic crossings of the n^*s state with many manifold states. Unlike in the n^*d data, the individual peaks are resolvable in this case because the avoided crossings are spaced farther apart. The minima due to different avoided crossings show a regular progression as the pulse amplitude increases. However, because all the pathways interfere at large principal quantum number there is no simple progression in the data.

In all of the data presented in Fig. 3, the experiments and calculations run in peak HCP voltage from below the first static-field crossing of the n^*s state with the manifold to above the manifold mixing region at $1/3n^5$. The results of the numerical simulations displayed in Fig. 3 were performed in the l basis for $|m_l|=0$ states using only the s state, the two nearest p states, and the nearest set of high-l states. Comparable calculations were done in the j basis and also using several adjacent sets of high-l states. Neither of these calculations showed any significant deviation from the simulations presented. The fact that there is no dependence on the difference between the l basis and the j basis is due to the fact that the spin-orbit coupling is much smaller than the HCP bandwidth, indicating that there is no mixing of these states during the HCP. The independence of the results from

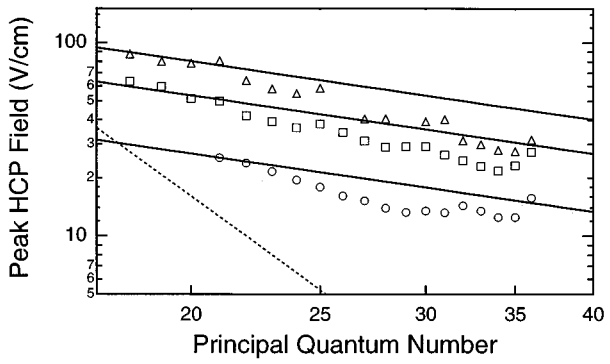

FIG. 6. Experimental (○) and theoretical field values for maxima in the population transfer between the initial n^*d state and the $l \geqslant 3$ states. The theoretical curves are based on a simple scaling argument about the quantum-mechanical phase of the states at the beginning and end of a pulse.

interaction with the adjacent manifolds is less easy to understand. It seems that when the pulse amplitude becomes large enough to reach $1/3n^5$, that the avoided crossings are all traversed nearly diabatically so that very little population reaches the avoided crossings at the manifold mixing field.

For the n^*d states it is possible to obtain a closed form expression for the phase defined in Eq. (5) with a few approximations in order to explore the coherence effects with the dynamic Stark model. If it is assumed that the energy levels are nearly hydrogenic, then the energy level difference in a field is given by $3nF$ and if the crossings are at zero (or small) field, then the integral of Eq. (5) can be carried out in closed form using pulse shape given in Eq. (1). This integral gives the result $\Delta\Phi = 9nF_0T/8$, where n is the principal quantum number. If $\Delta\Phi = 2\pi m$, where m is any integer, there will be constructive interference in the population transfer, giving rise to a minima in the initial-state population of Eq. (6). The above assumptions about the energy levels, pulse shape, and crossing locations determine that the peak field for the minima are

$$F_0 = \frac{16m\pi}{9nT}. \tag{7}$$

In Fig. 6 the fields at the first three maxima (discrete points) are plotted as well as the curve defined by Eq. (7) for $m = 1, 2, 3$. The agreement is good, with the data falling close to the lines, particularly at low n. The measured scaling of the different curves is $n^{-1.5}$ to $n^{-1.7}$, while the simple model predicts a scaling of n^{-1}. For the n^*s states, such a simple scaling argument is not possible, and the locations of the minima are only modeled successfully by the direct integration of the time-dependent Schrödinger equation.

These experiments show that within a single half-cycle of the field, that coherence must be taken into account. Over a wide range of avoided crossing size relative to the field frequency, the largest population transfer takes place when there is constructive interference between the two crossings and $P_{\text{diab}} \approx \frac{1}{2}$. We have shown that for properly chosen pulses, nearly 100% of the population can be redistributed.

B. Two HCP experiments

The data in Sec. III A have demonstrated that there are significant coherence effects in population redistribution within a single HCP. The Landau-Zener picture gives insight into the data and good agreement with the data for particularly simple cases. However, numerical integration is required to understand the situations where several states are involved and P_{diab} is large, since a change in the pulse amplitude implicitly alters both $\Delta\Phi$ and P_{diab}. A second experiment, which demonstrates the interference effect in a way that is much more straightforward to measure, involves applying a time-delayed pair of HCP's to the atoms. These experiments provide a direct measurement of the coherence of the redistribution process that is easily compared to theory.

With two HCP's, the population redistributed by a single HCP remains coherent at the end of the first pulse, and there is a well-defined phase difference between the populated states after the pulse. The phase of each state depends on its energy and evolves freely between two pulses. If a second HCP is incident on the atoms, population is again redistributed, and the final population depends both on the shape and amplitudes of the two pulses and the relative phase of the different states when the second pulse starts. The two-pulse field seen by the atoms can be expressed as

$$F_2(t) = F_1(t) + F_1(t-\tau), \tag{8}$$

where F_1 is defined in Eq. (1), and τ is the relative time delay between the two pulses. In a two-pulse experiment there are four avoided crossings like those seen in Fig. 4(b) which must be traversed, but the time between the pairs in each pulse are readily changed without affecting any other parameters of the population transfer. The relative phase accumulated between two states in the time interval between the initial and final crossings are

$$\Delta\Phi_{ij} = \frac{\Delta W_{ij}}{\hbar}\,\tau - \phi_{ij}, \tag{9}$$

where ΔW_{ij} is the zero-field energy level spacings, and ϕ_{ij} is a constant phase that depends on the pulse shape and amplitude. This allows the ready observation of coherence in the redistributed population using an interferometric technique.

In addition to measuring the coherence of the redistribution process, this interferometric technique is a powerful tool for spectroscopy in the range of MHz to THz. The Fourier transform of the interferogram determines the frequency intervals between states populated by the HCP's. The bandwidth available for spectroscopic measurements is orders of magnitude larger than the bandwidth of the pulses because of the high-order multiphoton nature of the transitions. Essentially we are using Stark shifts, which are usually a significant source of uncertainty in multiphoton spectroscopy, to our advantage. The highest frequency intervals that can be measured are only limited by the amplitude of the HCP's required to drive the transitions and stability of the pulse delay. Since the phases of Eq. (9) depend only on the relative pulse delay and the field free energies, the spectroscopic measurement is free from ac Stark shifts. The frequency resolution is only limited by the longest time delay available between the two pulses.

For weak-field interferometry, where the population transfer is described by first-order perturbation theory, the popu-

lation of each state will be modulated with the frequencies of the states that it interacts with. For nonperturbative HCP's, which are inherently used in these experiments, Jones *et al.* have demonstrated that the interferogram from a single bound state contains information about all bound levels populated during the HCP [24]. This means that the initial state should contain the frequency differences between all of the states that are populated by the HCP's.

Since the population transfers in the delayed-pulse experiments are strongly dependent on relative phase, and since the atomic frequencies are large compared to the HCP frequency, there must be good phase stability between the two HCP's. The phase jitter between the two pulses must be significantly less than the highest zero-field frequency differences, which are from 10 to 100 GHz for the states studied. For 100-GHz frequency differences a shot-to-shot jitter of 1 ps in time delay, which cannot be achieved electronically, is required. In order to create the two pulses, an arrangement similar to a Mach-Zehnder interferometer using coaxial microwave components, shown schematically in Fig. 1, was used.

Time delays between two pulses are generated by first splitting a single HCP using a Avtech Electrosystems AVX-SP-3 pulse power splitter. One of the pulses travels through a variable delay and the the two pulses are then recombined in an Avtech Electrosystems AVX-CP-1 pulse combiner. The variable delay is made with a trombone line (General Radio 847LTL) attached to a translation stage driven with a synchronous motor. With this scheme the relative delay between two pulses can be scanned by up to 1.4 ns with sub-ps phase stability. We increased the relative pulse delay by adding sections of low-loss coaxial cable to the leg of the interferometer containing the trombone line, allowing observation of the coherence as a function of delay over times longer than seen with the trombone line alone. This technique has allowed measurements of coherence for delays up to 20 ns. The translation stage is accurate to 0.25 mm over the full length, corresponding to an uncertainty of about 1 ps in the total delay. Since the trombone line has an air dielectric, relative time delays are readily determined from translation distance. Absolute delays are not so easily determined and can only be determined to within 0.25 ns by measurements made with a sampling oscilloscope. After the pulse is split and recombined, the maximum HCP amplitude is 40 V/cm in the interaction region.

In addition to stability in the relative pulse delay, the HCP amplitude stability must be good. The constant factor ϕ_{ij} in Eq. (9) depends on the HCP amplitude, and because the phase accumulated between the two pulses is approximately equal to the phase accumulated during each pulse, shot-to-shot fluctuations in the HCP amplitude can reduce the interference contrast.

Figure 7(a) shows the population in the 22d state as a function of relative pulse delay between 18 and 19.2 ns for HCP's with amplitudes of 18 V/cm. The absolute time scale is uncertain to about 0.25 ns, but this is unimportant since the signal is periodic. The modulation has a contrast of about 10%. Figure 7(b) shows a discrete Fourier transform of the data, which shows a single peak at 9.5 GHz. This corresponds to the frequency difference between the d state and the $n=22$ $l\geqslant 3$ states. In addition, there is a slow modulation

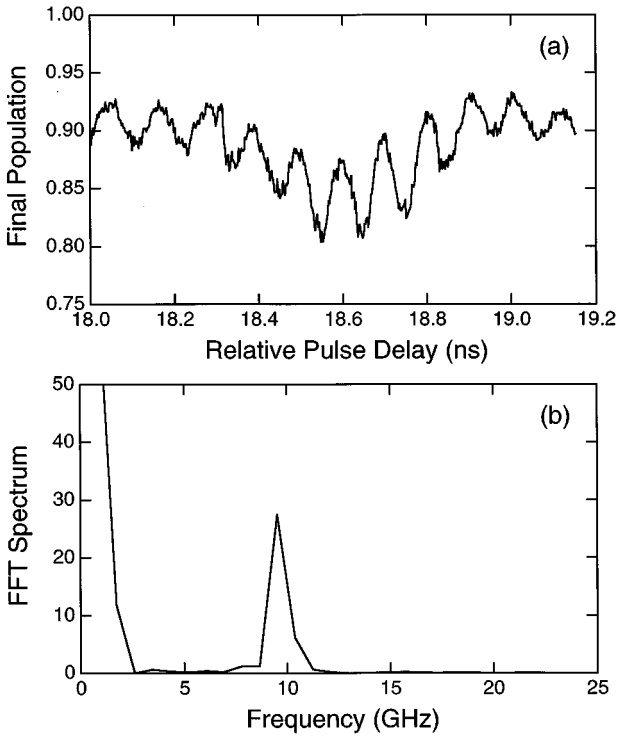

FIG. 7. Plots of (a) population in the 22d state as a function of relative pulse delay between two half-cycle pulses with an amplitude of 18 V/cm and (b) the power spectrum found by taking a discrete Fourier transform of the data in (a). A single peak appears, corresponding to the frequency between the 22d state and the $n=22l\geqslant 3$ states. The delay scan is not long enough to resolve the d-f and $d-$high-l frequencies.

of the data which, although it is not resolved in the Fourier transform, can be identified as an oscillation at the 22 f to $l\geqslant 3$ frequency difference of 0.9 GHz.

Figure 8 shows the somewhat more interesting scan of the delay between two pulses that drive transitions from the 33s state to the adjacent high-l states. The 33s population was measured as a function of relative pulse delay from about 10 to 11.5 ns for HCP's with an amplitude of 36 V/cm. These data again have a contrast of about 10%. The discrete Fourier transform of the data shows three frequencies. The two high frequencies 68.4 and 71.0 GHz, correspond to the transition frequencies between the 33s state and the 32d state and the 33s state and the $n^*=32$ $l\geqslant 2$ states. The lowest frequency, which would not exist if these were perturbative pulses, is the 32d to $n^*=32$ $l\geqslant 2$ frequency, 2.6 GHz.

Numerical simulations of the data shown in Figs. 7 and 8 were performed using the same methods as the simulations done for the scans of amplitudes shown in Figs. 3 and 4. The theory generally reproduces the data. For the n^*d states, the theoretical curves very closely match the experimental ones. For the n^*s states, the Fourier transform of the theoretical interferograms shows the same frequencies, but with somewhat different amplitudes. The contrast in the n^*s experiments is also lower than predicted by the theory, while for the n^*d states the contrast is very closely matched. The reduction in contrast between the numerical simulations and the experiments is likely due to a combination of field inhomogeneities within the interaction region and HCP amplitude

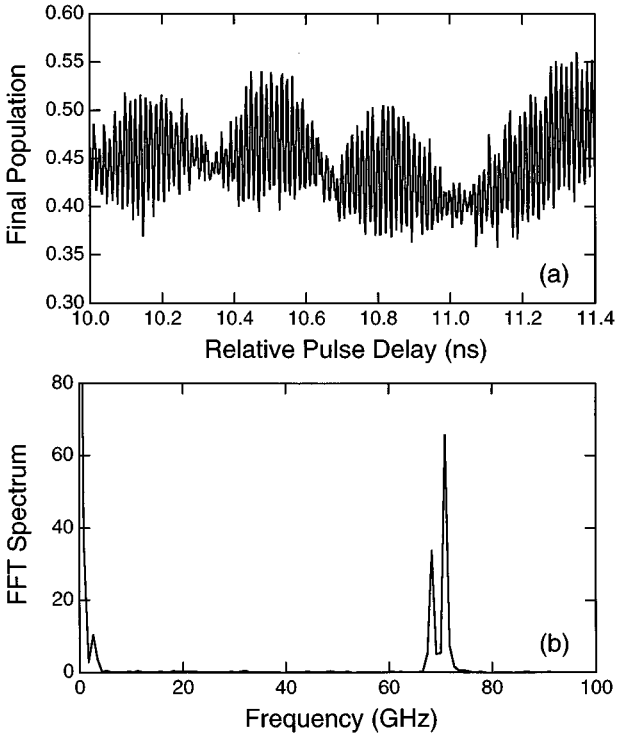

FIG. 8. Plots of (a) population in the 33*s* state as a function of relative pulse delay between two half-cycle pulses with an amplitude of 40 V/cm and (b) the power spectrum found by taking a discrete Fourier transform of the data in (a). Both the 33*s*-32*d* frequency, the 32*d*-$n=32$ $l\geqslant 3$ frequency, and the 33*s*-$n=32$ $l\geqslant 3$ frequency appear in the data. The existence of the *d*–high-*l* frequency shows that the results are nonperturbative.

jitter. It is likely that the deviations between the frequency spectrum between theory and experiment is due to the 7% reflected pulse or the long negative tail due to the low-frequency cutoff of the transmission line. Both of these effects can transfer population within the $l\geqslant 2$ states in the interval between the two pulses, affecting the measured interferogram.

These experiments show clearly and directly that the coherence is important in Rydberg-state populations distributed from n^*d and n^*s states by microwave HCP's and that the coherence persists for delays of up to 20 ns with little sign of damping in their amplitudes during this time delay. Because there is no static field present between the two pulses, none of the states are in the linear Stark regime, where small inhomogeneities in the field can cause dephasing over the volume of the atoms due to slightly different energies. For this reason we can see coherence for long-time delays between the pulses with little damping in their amplitudes.

IV. CONCLUSIONS

We have studied the coherent redistribution of populations between Rydberg states due to half-cycle pulses of microwave radiation with a coherent bandwidth significantly smaller than the spacing between states, but comparable to the sizes of the avoided crossings between the level-shifted states. This work demonstrates coherence among the redistribution of many Rydberg states by an HCP. Nearly 100% transfer of population was observed for certain amplitude HCP's, showing dramatically that only a few cycles are required to bring the onset of microwave ionization and that coherence effects are very important in these few-cycle experiments [11].

We have successfully used a Landau-Zener model that includes phase to describe the experiments in which two states are important and to give a qualitative understanding of the population transfer as a function of pulse amplitude and delay. Numerical integration of the time-dependent Schrödinger equation also quantitatively agrees with the results of the experiment. The level dynamics in this experiment are closely analogous to ac Stark-shifted multiphoton resonances and provide a clean experimental system on which to study nonperturbative dynamics.

In addition to measuring the coherence of the redistribution process, we have demonstrated an interferometric technique for multiphoton spectroscopy without ac Stark shifts. The bandwidth of the spectroscopy is significantly larger than the bandwidth of the pulses because of the multiphoton nature of the transitions. The highest frequencies that can be measured are only limited by the amplitude of the HCP's required to drive the transitions and the frequency resolution is only limited by the longest time delay available between the two pulses, which could easily be increased over the range used in this experiment by using several trombone lines in parallel. This method is also readily usable for lower frequencies, in the MHz to GHz range, with electronically controlled delays between two pulses. We are currently exploring ways to make the interferometric technique demonstrated into a viable spectroscopic technique.

HCP's populate many high-*l* states, and form angular wave packets. For short enough pulses, experiments using n^*d states produce distributions of high-*l* states that are similar to states that exist in a static field (the parabolic states). These wave packets would have a permanent dipole moment in zero field. An interesting application of such a transition would be to create a radial wave packet of n^*d states and then apply a HCP to drive the n^*d states into the superposition state of high-*l* states with multiple principal quantum numbers. Such a wave-packet state would be localized in three dimensions. Additionally, the influence of noise on microwave multiphoton transitions and microwave ionization has been the subject of recent experiments [25–26]. It would be useful to apply different noise signals between the two HCP's to perform a more controlled experiment on these effects. Finally we are looking at the application of several microwave HCP's to place the transferred population into a specified final state.

ACKNOWLEDGMENTS

We would like to thank both Robert Jones and Philip Bucksbaum for many useful discussions. Philip Bucksbaum is also thanked for the loan of the trombone line. Acknowledgment is made to the donors of the Petroleum Research Fund, administered by the ACS, for partial support of this research. This work was partially supported by Research Corporation. J.H.R. was supported by a grant from Colby College.

[1] P. Brumer and M. Shapiro, Chem. Phys. Lett **126**, 541 (1986); M. Shapiro and P. Brumer, J. Chem. Phys. **97**, 6259 (1992); W. S. Warren, H. Rabitz, and M. Dahleh, Science **259**, 1091 (1995).

[2] P. Pillet, C. Valentin, R.-L. Yuan, and J. Yu, Phys. Rev. A **48**, 845 (1993).

[3] T. F. Gallagher, L. M. Humphrey, W. E. Cooke, R. M. Hill, and S. A. Edelstein, Phys. Rev. A **16**, 1098 (1977).

[4] M. G. Littman, M. M. Kash, and D. Kleppner, Phys. Rev. Lett. **41**, 103 (1978).

[5] T. H. Jeyes, G. W. Foltz, K. A. Smith, E. J. Beiting, F. G. Kellert, F. B. Dunning, and R. F. Stebbings, Phys. Rev. Lett. **44**, 390 (1981).

[6] J. E. Bayfield and P. M. Koch, Phys. Rev. Lett. **33**, 258 (1974).

[7] P. Pillet, W. W. Smith, R. Kachru, N. H. Tran, and T. F. Gallagher, Phys. Rev. Lett **50**, 1043 (1983); P. Pillet, H. B. van Linden van den Heuvell, W. W. Smith, R. Kachru, N. H. Tran, and T. F. Gallagher, Phys. Rev. A **30**, 280 (1984).

[8] R. R. Jones, D. You, and P. H. Bucksbaum, Phys. Rev. Lett. **70**, 1236 (1993); N. E. Tielking and R. R. Jones, Phys. Rev. A **52**, 1371 (1995); N. E. Tielking, T. J. Bensky, and R. R. Jones, *ibid.* **51**, 3370 (1995).

[9] G. M. Lankhuijzen and L. D. Noordam, Phys. Rev. Lett. **74**, 355 (1995); **74**, 3305(E) (1995).

[10] M. T. Frey, F. B. Dunning, C. O. Reinhold, and J. Burgdörfer, Phys. Rev. A **53**, R2929 (1996); C. O. Reinhold, J. Burgdörfer, M. T. Frey, and F. B. Dunning, *ibid*. **54**, R33 (1996).

[11] M. Gatzke, B. Broers, L. D. Noordam, R. B. Watkins, and T. F. Gallagher, Phys. Rev. A **50**, 2502 (1994).

[12] R. R. Freeman, P. H. Bucksbaum, H. Milchberg, S. Darack, D. W. Schumacher, and M. E. Geusic, Phys. Rev. Lett. **59**, 1092 (1987).

[13] M. P. de Boer and H. G. Muller, Phys. Rev. Lett. **68**, 2747 (1992); M. P. de Boer, L. D. Noordam, and H. G. Muller, Phys. Rev. A **47**, R45 (1993).

[14] J. G. Story, D. I. Duncan, and T. F. Gallagher, Phys. Rev. Lett. **70**, 3012 (1993); Phys. Rev. A **50**, 1607 (1995).

[15] R. B. Vrijen, J. H. Hoogenraad, H. G. Muller, and L. D. Noordam, Phys. Rev. Lett. **70**, 3016 (1993); R. B. Vrijen, J. H. Hoogenraad, and L. D. Noordam, Mod. Phys. Lett. B **8**, 205 (1994).

[16] R. R. Jones, Phys. Rev. Lett. **74**, 1091 (1995).

[17] M. L. Zimmerman, M. G. Littman, M. M. Kash, and D. Kleppner, Phys. Rev. A **20**, 2251 (1979).

[18] C. J. Lorenzen and K. Niemax, Phys. Scr. **27**, 300 (1983).

[19] W. H. Press, B. P. Flannery, S. A. Teukolsky, and W. T. Vetterling, *Numerical Recipes* (Cambridge University Press, Cambridge, 1986).

[20] J. R. Rubbmark, M. M. Kash, M. G. Littman, and D. Kleppner, Phys. Rev. A **23**, 3107 (1981).

[21] T. J. McIlrath, R. R. Freeman, W. E. Cooke, and L. D. van Woerkom, Phys. Rev. A **40**, 2770 (1989); L. D. van Woerkom, R. R. Freeman, W. E. Cooke, and T. J. McIlrath, J. Mod. Opt. **36**, 817 (1989).

[22] M. Gatzke, R. B. Watkins, and T. F. Gallagher, Phys. Rev. A **51**, 4835 (1995).

[23] I. A. Komarov, T. P. Grozdanov, and R. K. Janev, J. Phys. B **13**, L573 (1980).

[24] R. R. Jones, C. S. Raman, D. W. Schumacher, and P. H. Bucksbaum, Phys. Rev. Lett. **71**, 2575 (1993).

[25] S. Yoakum, L. Sirko, and P. M. Koch, Phys. Rev. Lett. **69**, 1919 (1992).

[26] O. Benson, A. Buchleitner, G. Raithel, M. Arndt, R. N. Mantegna, and H. Walther, Phys. Rev. A **51**, 4862 (1995).